Predicting scale-dependent chromatin polymer properties from systematic coarse-graining

Sangram Kadam,[1,*] Kiran Kumari,[1] Vinoth M,[1] Shuvadip Dutta,[2] Mithun Mitra,[2] and Ranjith Padinhateeri[1,†]

[1] *Department of Biosciences and Bioengineering, Indian Institute of Technology Bombay, Mumbai 400076, India*
[2] *Department of Physics, Indian Institute of Technology Bombay, Mumbai 400076, India*

Simulating chromatin is crucial for predicting genome organization and dynamics. Even though coarse-grained bead-spring polymer models are commonly used to describe chromatin, the relevant bead dimensions and elastic parameters are unknown. Using publicly available nucleosome-resolution contact probability (Micro-C) data, we systematically coarse-grain chromatin and predict quantities essential for polymer representation of chromatin. We compute size distributions of chromatin beads for different coarse-graining scales, quantify fluctuations and distributions of bond lengths between neighboring regions, and derive effective spring constant values. Unlike the prevalent notion, our findings argue that coarse-grained chromatin beads must be considered as soft particles that can overlap, and we propose an overlap parameter. We also compute angle distributions between neighboring bonds giving insights into intrinsic folding and local bendability of chromatin. While nucleosome-linker DNA bond angle naturally emerges from our work, we show that there are two populations of local structural states. The bead sizes, bond lengths, and bond angles show different mean behavior at Topologically Associating Domain (TAD) boundaries and TAD interiors. Our findings provide important insights for building coarse-grained chromatin models that are consistent with different physical properties.

PACS numbers:

Introduction

The eukaryotic genome is organized in the form of many long chromatin polymer chains, each essentially a string of nucleosomes—DNA wrapped around histone proteins—folded, looped, and condensed into domains of different compaction [1–4]. The spatial and temporal organization of these chains and their internal epigenetic states are crucial in deciding aspects ranging from cellular function to differentiation and development [5–8].

Chromosomes are typically simulated and studied as coarse-grained(CG) bead-spring polymer chains. A coarse-grained polymer picture is useful for many reasons: it is nearly impossible to simulate the huge polymer set (∼millions of nucleosomes) in its entirety. More importantly, the coarse-grained representation, with effective parameters, can be a powerful tool to understand chromatin organization and dynamics and make useful predictions [9–22]. However, since we still do not understand the chromatin structure and properties in detail, systematic coarse-graining has been a difficult task. We do not fully know the polymer properties/parameters relevant for coarse-grained chromatin.

Owing to a large body of work over the past few decades, double-stranded DNA has a good coarse-grained description as a semi-flexible polymer [23–25]. We understand its coarse-graining size, bending stiffness, stretching elasticity, and other relevant parameters [24, 25]. However, chromatin is a more complex polymer having heterogeneous properties arising from different epigenetic states, amount of different proteins bound, and local folding [26, 27]. This complexity makes it difficult to accurately compute coarse-grained bead diameter, elastic constants, and other physical properties for a chromatin polymer.

Recent experimental advances have made it possible to understand chromatin structure using biochemical methods like Hi-C, Micro-C [28–37] and imaging methods like SAX, cryo-EM, and super-resolution imaging [38–45]. The studies so far show that chromatin is organized into different compartments and topologically associated domains (TADs) [2, 7, 29–31]. While histone modifications, transcription factors, and chromatin binding proteins greatly affect chromatin folding and make it a highly heterogeneous polymer, how the interplay between these factors decides the compaction and dynamics of chromatin is currently being investigated.

While different experimental methods provided us data to understand chromatin organization [28–31, 33–35, 38–40, 42–44, 46, 47], theoretical/computational studies have been pivotal in understanding and explaining chromatin characteristics [9–13, 16–20, 22, 48–62]. Models that simulated chromatin at nucleosome resolution primar-

*Electronic address: sangramkadam@iitb.ac.in
†Electronic address: ranjithp@iitb.ac.in

ily investigated how different molecular interactions influenced higher-order organization beyond the 10nm chromatin [49, 51, 52, 57, 62–65]. Nearly all models that are employed to understand Hi-C/microscopy data represented chromatin as a bead-spring polymer chain with each bead representing chromatin of length in the range $\sim$ 1kb to 1Mb [10–15, 18–22]. However, physical dimensions and elastic properties of chromatin are not well understood. What is the diameter of a 1kb, 10kb or 100kb chromatin bead? What is the magnitude of the spring constant that would represent the thermal fluctuation of chromatin at different length scales? Should chromatin be considered a flexible polymer or a semi-flexible polymer? Does it have an intrinsic curvature/bending stiffness? None of these questions have clear, definitive answers in the literature, currently. While it is well known that chromatin behavior is heterogeneous, depending on the epigenetic state, existing coarse-grained models of chromatin typically assume that the physical dimensions of the beads and elastic properties of the filament are uniform along the polymer, independent of the epigenetic state. How these properties—size of the beads, stretching elasticity, bending elasticity, etc.—vary along the contour is also unknown. In the current models, the heterogeneity of chromatin is often incorporated into additional intra-chromatin interactions—interaction between two far-away beads [10, 22, 66]. Since one does not know the size of a coarse-grained chromatin bead, it is taken as a fitting parameter—a constant number across the filament—to achieve experimentally measured 3D distance values [10, 13, 20, 22, 67, 68]. Fig. S1 shows some of the reported values and how scattered they are. We do not understand this variability and what each number means.

One could not do systematic coarse-graining so far because the chromatin conformation capture data was available only with lower resolutions like 100kb, 10kb, and up to 1kb [28–31, 46]. Obtaining information smaller than the HiC resolution was not possible. Moreover, even at the smallest size scale ($\sim$ kb), the physical dimension of chromatin—chromatin bead diameter—was an unknown parameter. However, recent experiments have provided us chromatin conformation capture data at near-nucleosome resolution—200 bp resolution, which is essentially a nucleosome plus the linker DNA [32, 33, 37]. This data enables us to make a fine-grained (FG) chromatin model and systematically probe the properties of the coarse-grained chromatin. The advantage here is that the physical size of a 200bp chromatin is not a completely unknown free parameter; we do have a fair idea about the size of a 200bp chromatin bead. In this work, we take advantage of this recent fine-grained data, start from the 200bp Micro-C contact map, and construct chromatin polymer configurations that satisfy the map. From our work, without any arbitrary fitting parameter, the 3D distances and radius of gyration values emerge in a reasonable range comparable to known experiments. Using the 200bp-chromatin as a fine-grained polymer, we coarse-grain the chromatin systematically. This enables us to predict several quantities essential for anyone simulating a coarse-grained chromatin polymer. We predict (i) the physical sizes of coarse-grained beads of various chromatin length scales, (ii) the overlap between coarse-grained beads, (iii) the value of the spring constant between neighboring beads dictating the fluctuation, and (iv) the distributions of bond angles and dihedral angles giving insights into the stiffness of chromatin. We demonstrate that some of the ideas we learned—e.g., soft inter-bead interactions that allow overlap—are crucial for obtaining sensible 3D distances when coarse-grained models are employed.

Model and Methods

Model-I. Fine-grained chromatin model with 200bp resolution chromatin: Our basic model is the fine-grained (FG) chromatin polymer model with 200bp resolution, constructed based on the publicly available Micro-C data for mouse embryonic stem cells (mESCs) [33, 34]. The polymer is made of N spherical beads, having the size of 200bp chromatin (diameter σ), with nearest-neighbor connectivity via harmonic springs and self-avoiding interaction via the repulsive part of the Lennard-Jones potential (see Fig. 1(a), Supplementary Information (SI) Sec. S1.A). Since each bead consists of a nucleosome and 50bp linker DNA, we call the bead a "nucleosome-linker" (NL) bead. To generate an ensemble of configurations consistent with Micro-C data, we connected (brought into proximity) bead pairs i and j with the experimentally observed contact probability P_{ij} in a two-step process. First, we defined a set of prominent (strong) contacts of the Micro-C contact map (see Sec. S1.A) [66]. Taking only the prominent contact probability values, we inserted harmonic springs between bead pairs i and j if $r_n < P_{ij}$, where r_n is a uniformly distributed random number between 0 and 1. We generated 1000 independent polymer configurations using this procedure and equilibrated them using Langevin simulations with LAMMPS [69]. We defined "prominent contacts" as follows [66]: Since the contact map depends only on $|i-j|$ for homogeneous polymers, we took the set of all P_{ij} values for a given $|i-j|$ and computed their mean and standard deviation. If P_{ij} was at least one standard deviation larger than the mean, we considered it as a prominent contact (see SI). Prominent contacts are defined for each $|i-j|$ line in the matrix (line parallel to the diagonal representing all equidistant bead pairs). Bonding prominent contacts ensured that all actively acquired far away contacts (e.g., contacts via loop extrusion) were present.

In the second step, going beyond the prominent contacts, our aim is to insert contacts in the P_{ij} fraction of the configurations (out of the 1000 configurations) for each bead pair (i, j). To achieve this, we started with the ensemble of equilibrated configurations from step-1 and inserted harmonic springs between beads i and j in the P_{ij} fraction of

configurations whose 3D distances (r_{ij}) are the smallest (see SI). This system was then equilibrated using Langevin simulations with LAMMPS. While the first step ensured that the configurations are influenced by strong contacts formed via events like loop extrusion, the second step ensured that all bonds closer in space would have priority in forming protein-mediated contacts.

We have used the minimal FG model that accounts for polymer connectivity, self-avoidance, and contact probability. The assumption here is that all other properties of the FG polymer (like inter-nucleosome interactions and stiffness) lead to the experimentally observed contact probability, which we have ensured. Our model generates all possible polymer configurations such that the experimentally known constraint of the contact map is satisfied.

Size of a 200bp chromatin bead (σ): Since a 200bp chromatin bead is bigger than a nucleosome, its size has to be greater than the size of the nucleosome (11nm) [3]. As geometrically shown in Fig. S2(a), since two neighboring nucleosomes are connected via a rigid 50bp linker DNA, the distance between them can be $\approx$ 28nm. However, two far-away nucleosomes can come as close as 11–12nm (with histone tails and other bound proteins). Hence, on average, one expects an effective size $\approx$ 20nm. In the Results section, we have shown that when $\sigma = 21$nm, the 3D distances, and R_g values match well with experimental data. This is also consistent with the earlier observation that $\sigma = 25$nm for 250bp beads [67].

Since the Model-I did not have explicit linker DNA, we also simulated short chromatin with nucleosomes, explicit linker DNA, and entry–exit angles between nucleosomal DNA. In this detailed Model-II, the chromatin polymer has two types of beads—linker DNA bead and nucleosome bead (see Sec. S1.B)[70]. In the Results section, we have compared the radius of gyration of chromatin segments from Model-II and the first fine-grained model. This also suggests that our $\sigma = 21$nm value is indeed reasonable.

Results and Discussion

Constructing 3D chromatin configurations at near-nucleosome resolution consistent with Micro-C contact map and measured 3D distances

We simulated a fine-grained chromatin polymer made of "nucleosome-linker" (NL) beads, with each bead representing 200bp of chromatin (Fig. 1(a), Methods and SI), and generated an ensemble of steady-state chromatin configurations, taking the Micro-C contact probability data (P_{ij}) of mouse embryonic stem cells (mESCs) as input [33]. We simulated a euchromatic (Chr 5: 31.17 Mb to 31.25 Mb, $N = 400$) and a heterochromatic (Chr 7: 70.24 Mb to 70.4 Mb, $N = 800$) region. We computed the ensemble-averaged contact probability for both regions and compared it with the input contact map. The contact maps from the simulations appear visually similar to the Micro-C data (Fig. 1(b–e)). We quantified the similarity by computing the Pearson's correlation coefficient, which is 0.88 and 0.85 for the two regions (Fig. S2(d)). We have also done a similar exercise for mESC alpha-globin region (Fig. S2(c)). We then computed the mean 3D distances between different segments of all these polymers. As shown in Fig1(f) (for alpha-globin region), the mean 3D distance from our simulations is comparable to what is observed in experiments [10, 71].

We now systematically coarse-grain all the above chromatin polymers. We chose n_b consecutive NL beads to form a coarse-grained CG bead (colored big bead in Fig. 2(a) top right). The coarse-grained polymer consists of N/n_b number of CG beads. We then measured various properties of the coarse-grained polymer such as size of the CG bead R_g, bond length $l_{\rm cg}$, bond angle $\theta_{\rm cg}$ (Fig. 2(a) bottom), and dihedral angle $\phi_{\rm cg}$ (Fig. 4(a) bottom). We study how these properties depend on the coarse-graining size n_b and the genomic location. As a control, we have compared our chromatin results with the ideal chain (bead spring polymer with no self-avoiding interaction), the SAW (Self Avoiding Walk; bead spring polymer with Weeks–Chandler–Anderson potential), and a highly packed globule (bead spring polymer with attractive Lennard-Jones potential with $\epsilon = 1k_B$T).

Predicting the size of a coarse-grained chromatin bead, and its variability along the genome

Since nearly all polymer simulations use coarse-grained beads of various genomic lengths like 1kb, 10kb, 100 kb, etc., it is important to understand the physical size (radius) of such a coarse-grained bead. Does bead size depend on the state of the chromatin (heterochromatin or euchromatin) and/or the genomic location of the bead (TAD interior, TAD boundaries)? To answer this, we first computed the radius of gyration (R_g) of the n_b consecutive beads that form a CG bead. Taking a sliding window of n_b beads, we plotted the average radius of gyration (R_g^i) as a function of genomic location (Fig. 2(b) and Fig. S3(a); real units in X_2 and Y_2 axes). For both euchromatic and heterochromatic segments, R_g values vary along the genomic length for the same coarse-graining, representing heterogeneities along the chromatin. In contrast, R_g curves for SAW and packed globule do not vary along the polymer contour (Fig. S3(b)

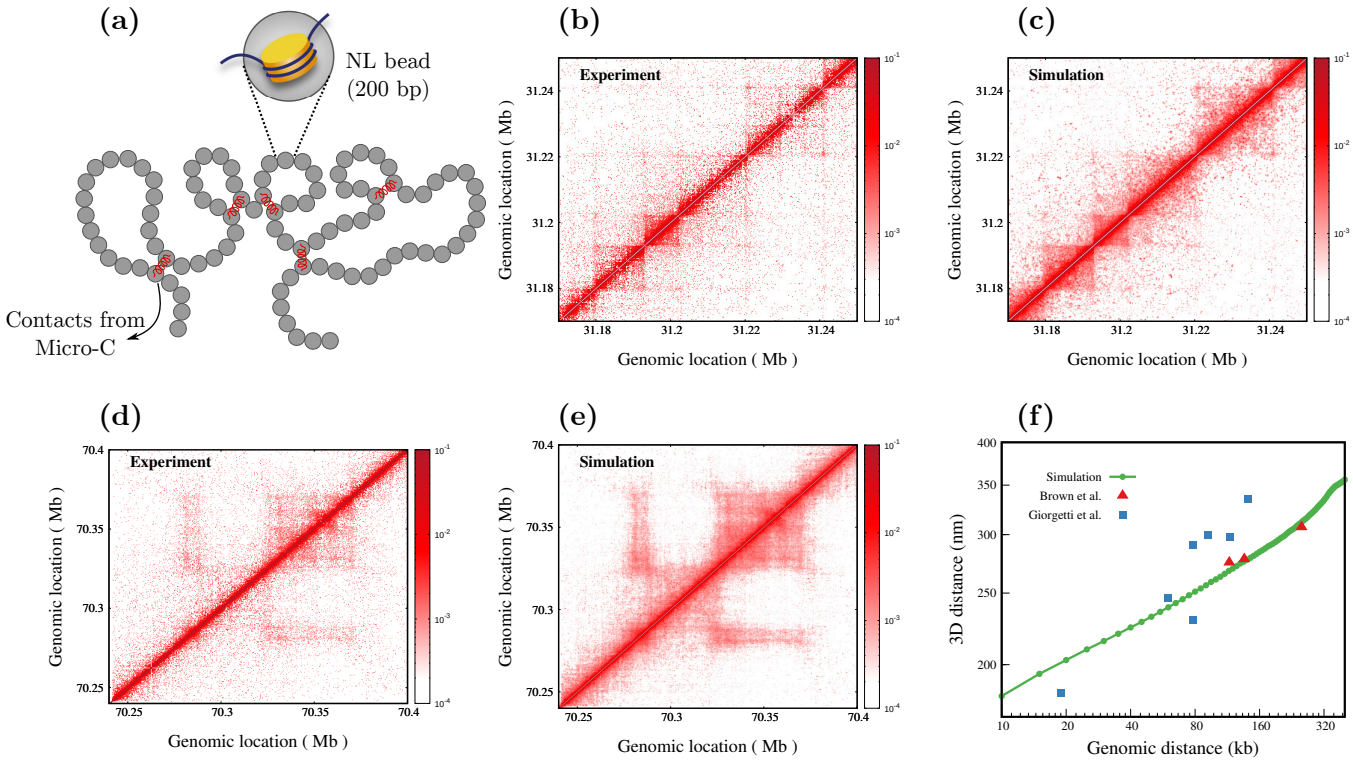

FIG. 1: Chromatin configurations consistent with experiments: (a) Schematic of the fine-grained (FG) chromatin polymer with one bead representing 200bp nucleosome+linker (NL) chromatin. An ensemble of configurations are generated such that any pair of beads (i, j) is connected(red springs) with a probability p_{ij}, based on observed contacts in Micro-C experiments (see text). (b–e): Comparison of contact maps obtained from our simulation to experiments for a euchromatic region (b–c), and a heterochromatic region(d–e). (f) 3D distance from our alpha globin simulation (green filled circles) compared with available experimental data for the same region (red filled triangles) taken from Brown et al. [71], and other regions (blue squares) of similar genomic length range taken from Giorgetti et al. [10].

and (c)). To understand how the locations of the peaks and troughs in the R_g correlate with the contact map, we compared them in Fig. 2(c) for a 1kb coarse-graining scale. R_g values peak at the TAD boundaries and are relatively small within the interior of each TAD. That is, coarse-grained beads representing inter-TAD regions will have a larger physical dimension. This is consistent with what is observed in recent experiments [38].

How big is a typical 1kb, 5kb or 10kb chromatin? We compared the mean R_g values (averaged over the entire region we considered) for a euchromatic and a heterochromatic region (Fig. 2(d)) along with SAW polymer for reference. A one kb euchromatic region has an $R_g \approx 25$nm, while for a 10 kb region we obtain $R_g \approx 85$nm. Depending on the precise nature of the epigenetic state, the R_g value for 10kb may have a wide range from ≈ 70 to 120 nm (close packing to SAW). To check whether our predictions are roughly of the same order as what is seen in experiments, we compared them with experiments that measured R_g [43] (data points Fig. 2(d)). Although the experimentally known R_g values are for a different cell type, they do indeed fall in the range that we are predicting, suggesting that R_g values from our simulation are reasonable. In Fig. S3(d–e) we also show the distribution of R_g values.

To independently check the order of magnitude of R_g values, we employed another realistic, detailed model of short chromatin with explicit nucleosomes having entry/exit angles and linker DNA explicitly (Fig. S2(b) and Sec. S1.B). We find that the size of a 1kb chromatin made of 5 nucleosomes in this model is comparable to what we predict using our basic fine-grained model (Fig. S2(f)), suggesting that the FG model we use is reasonable.

Coarse-grained chromatin beads are not hard spheres; they overlap impacting bond length and stiffness

For a long polymer that can mix, another equally important quantity is the distance between the centers of two neighboring coarse-grained beads, defined as the bond length $l_{\rm cg}$, depicted in Fig. 2(a). In Fig. 3 we present the bond length, its statistics, and the stretching elastic constants derived from it. First, mean $l_{\rm cg}$ values vary depending

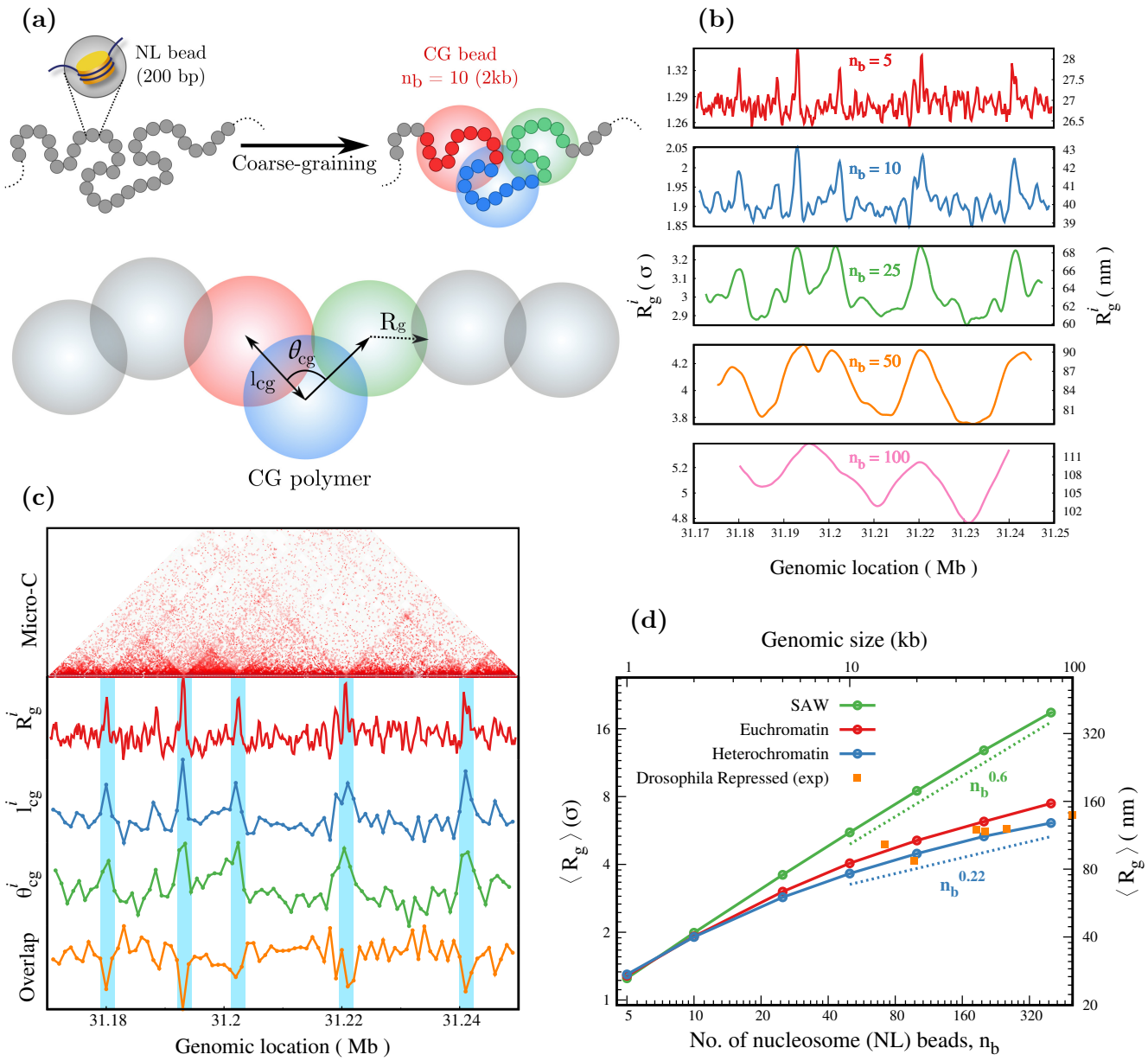

FIG. 2: (a) Schematic showing the coarse-graining procedure and quantities of interest. The fine-grained polymer of N beads (grey, small beads, representing 200bp of nucleosome+linker (NL)) is coarse-grained into N_{cg} big beads, with each big coarse-grained bead containing $n_b = N/N_{cg}$ beads. For illustration purposes, ten small colored beads ($n_b = 10$) are coarse-grained into one big CG bead. $l_{\rm cg}$ is the length of the bond connecting two successive coarse-grained beads, $\theta_{\rm cg}$ is the angle between two successive bonds, and R_g is the radius of gyration of the coarse-grained polymer segment of size n_b. (b) Average radius of gyration at different genomic locations (R_g^i) for different n_b values for a euchromatic region (Chr 5). (c) Variation of R_g^i and other quantities (l_{cg}^i, θ_{cg}^i, and overlap, see text) along the chromatin contour ($n_{\rm b}$=5). Note different behavior at the TAD boundaries (vertical strip) and TAD interiors. (d) Mean R_g for different coarse-graining sizes (n_b) showing the predicted range of values for different chromatin states. Data points are experimental data from Boettiger et al. [43] to demonstrate that the R_g values predicted are reasonable. Dotted lines are shown as guide to the eye. R_g values are presented in the units of NL bead size σ (Y_1 axis) and also in nm (Y_2 axis).

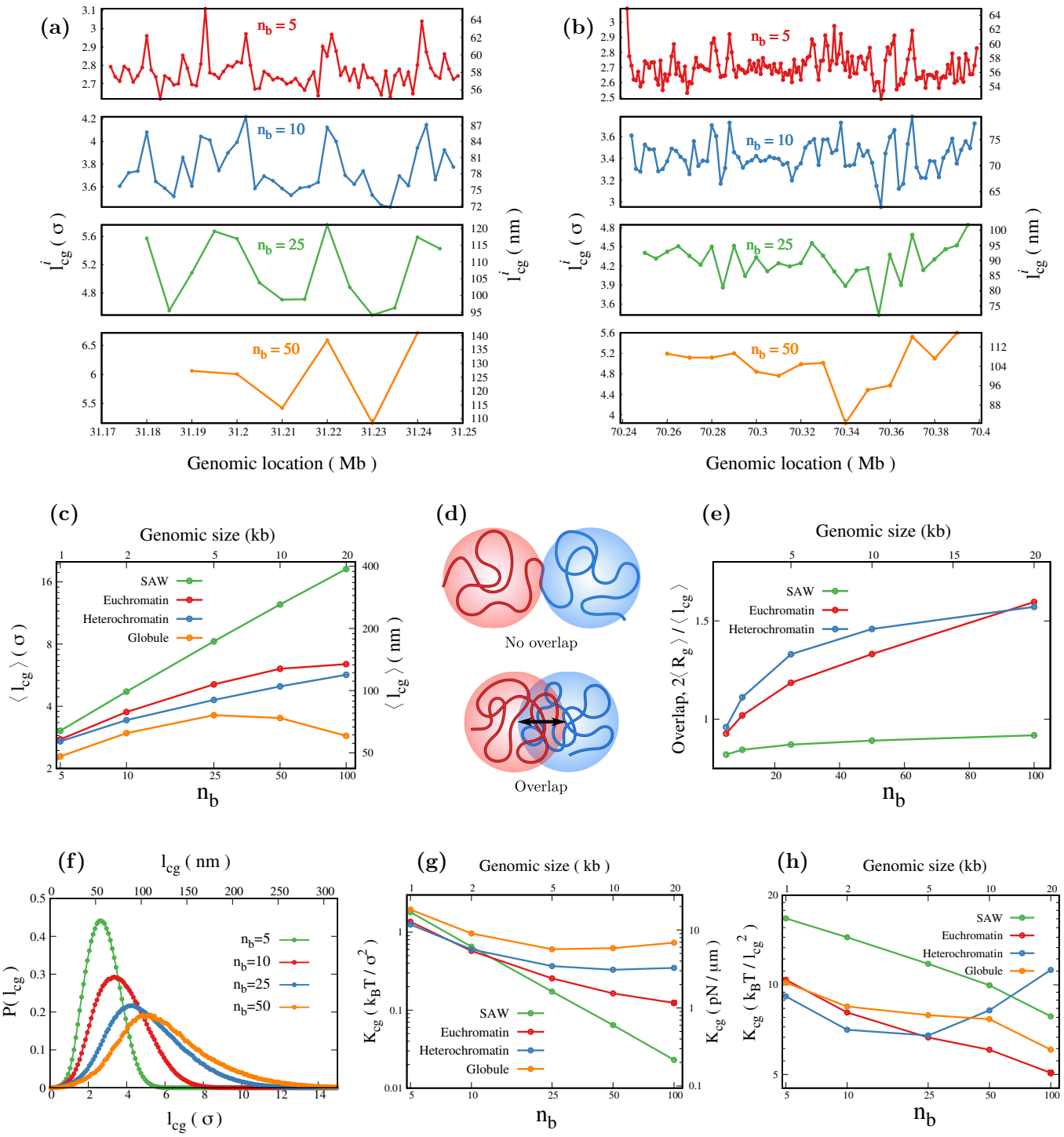

FIG. 3: Spatial variation of average bond length (l^i_{cg}) for different coarse-graining sizes (n_b), for (a) euchromatic, and (b) heterochromatic regions. (c) Average l_{cg} for different coarse-graining sizes showing the range of values possible from SAW to globule; presented in two different units in Y_1 and Y_2 axes. (d) Schematic showing two nearby long polymer segments "mixing" (or not mixing) in 3D space resulting in overlap (or no overlap) of coarse-grained (colored) beads. (e) A parameter that quantifies the extent of overlap is plotted for different n_b values. (f) Distribution of l_{cg} for euchromatin region. (g–h) The effective spring constant (K_{cg}) quantifying the fluctuation between neighboring coarse-grained beads for chromatin segments in different epigenetic states, presented in two different units. CG simulations would need units in (h).

on the coarse-graining size and genomic location both for euchromatin and heterochromatin (Fig. 3(a) and (b)). Similar to R_g, the bond length is also high at certain genomic locations like TAD boundaries and low in the TAD interiors (Fig. 2(c)). This is essentially the same behavior found in recent experiments [38], which showed that the inter-TAD distances are larger than the intra-TAD distances, consistent with the spatial variation in coarse-grained bead sizes observed in our simulations. Given that a typical chromatin polymer will contain both euchromatic and heterochromatic regions, it is instructive to compare extreme sizes of coarse-grained beads to understand the variability one can expect along the genome. For a 5kb segment ($n_{\rm b}$= 25), the mean $l_{\rm cg}$ values at different genomic locations vary between $\approx$ 70nm (heterochromatin) to $\approx$ 120nm (euchromatin)—compare $n_b = 25$ in Fig. 3(a) and (b). This implies that real chromatin will have highly heterogeneous bead dimensions, unlike the prevalent uniform bead size picture. The mean values of bond length, averaged over all genomic locations, are shown as a function of n_b (coarse-graining scale, genome size) for euchromatin and heterochromatin (Fig. 3(c)). Similar coarse-grained bond lengths for SAW and globule are shown as control. Heterochromatin has, as expected, a smaller bond length compared to euchromatin.

How is $l_{\rm cg}$ related to R_g? Naively one would expect that $l_{cg} \approx 2R_g$. However, this is not the case; chromatin has $l_{cg} < 2R_g$ because the two nearby polymer segments can "mix"—CG beads can overlap—and have their center of mass locations nearby (Fig. 3(d)). To quantify the overlap or mixing between the two adjacent coarse-grained beads, we define an overlap parameter $\mathcal{O} = (2R_g/l_{cg})$ (Fig. 3(e)). If the coarse-grained regions are perfectly spherical and non-overlapping(no mixing) $\mathcal{O} = 1$. For SAW, $\mathcal{O} < 1$ and is nearly independent of coarse-graining scale (n_b). For euchromatin and heterochromatin $\mathcal{O} > 1$ (i.e., $l_{cg} < 2R_g$) implying the mixing of adjacent polymer segments. We also find that $\mathcal{O}$ depends on the coarse-graining scale. Since $l_{cg} \neq 2R_g$, should one consider $l_{\rm cg}$ as the size (diameter) of an effective coarse-grained bead, or $2R_g$? This is a relevant question for coarse-graining; given the fact that the beads can overlap, we propose that $l_{\rm cg}$ may be considered as the effective diameter of a coarse-grained bead. We also computed $\mathcal{O}$ a function of genomic location (Fig. S4(d)). Comparing the overlap with the contact map shows that the TAD boundary locations have a smaller overlap than the TAD interior; even though the boundary regions have larger bead sizes (R_g), the mixing between neighboring beads is lower (Fig. 2(c)).

Going beyond the average size, we computed the bond length distribution $P(l_{cg})$ that has all the information about the fluctuation and higher moments. As a control, for the ideal polymer chain, $P(l_{cg})$ from the simulation matches with the analytical relation proposed by Laso et al. [72](Fig. S4(a)). We then plot $P(l_{cg})$ for euchromatin and heterochromatin for different coarse-graining sizes (Fig. 3(f) and Fig. S4(b)). From the distribution, we can derive an effective potential energy $V(l_{cg}) = -k_{\rm B}T \ln P(l_{cg})$ with which two neighboring beads interact. Even though the distribution is not perfectly Gaussian, a measure of the elastic constant of the interaction can be computed from the inverse of the standard deviation. Hence, we define an effective spring constant between two neighboring CG beads as $K_{cg} = \frac{k_B T}{\langle l_{cg}^2 \rangle - \langle l_{cg} \rangle^2}$, where the angular brackets indicate the average computed using $P(l_{cg})$. In Fig. 3(g), we plot K_{cg} for different coarse-graining sizes and epigenetic states. The spring constant is scale dependent—it decreases as the coarse-graining size increases, for SAW and euchromatin, indicating more fluctuations when the coarse-graining size is large.

For heterochromatin and globule, the spring constant values appear to saturate at a large coarse-graining scale, unlike the SAW polymer. The K_{cg} value for large n_b is in the range (0.1–1) $k_{\rm B}T/\sigma^2$, which is $\approx$ (1–10) pN/μm. This value is roughly comparable to some of the experimentally measured values from pulling long chromatin under certain in vitro conditions [73]. Note that, in contrast to pulling experiments where external forces can disrupt protein-mediated interactions, our estimate of the spring constant arises purely from thermal fluctuations and is thus expected to be a reliable signature of chromatin flexibility. Moreover, this is for relatively more dynamic MESc; hence the chromatin stretching stiffness obtained here will be less than that from the pulling experiments of mitotic chromosomes [74].

The spring constant above is presented in units of k_BT/σ^2 where σ is the size of a 200bp NL bead. However, in coarse-grained polymer simulations, one uses K_{cg} in units of k_BT/l_{cg}^2. Since $l_{\rm cg}$ also depends on CG size (n_b), the spring constant has a non-trivial behavior and is presented in Fig. 3(h). This gives a very useful range of numbers that can be used in all future coarse-grained simulations as K_{cg} = 5–10 k_BT/l_{cg}^2 for coarse-grained beads of size 1–20kb.

Predicting angle distribution and stiffness between neighbouring coarse-grained chromatin segments

How flexible is a chromatin polymer segment? Do chromatin polymer segments have intrinsic curvature? While we understand the bendability of DNA reasonably well, we know very little about the bending elastic behavior of chromatin. From the large ensemble of structures that we have produced, consistent with nucleosome level Micro-C data, we computed the distribution of: the bond angle ($\theta_{\rm cg}$)—angle between two neighboring bonds connecting three consecutive CG beads (see Fig. 4(a) top), and the dihedral angle ($\phi_{\rm cg}$)—angle between two neighboring planes formed by three consecutive bond vectors (Fig. 4(a) bottom).

The bond angle is defined as $\theta_{cg} = \pi - \alpha$, where $\alpha = \cos^{-1}(\hat{l}_{cg}^{i} \cdot \hat{l}_{cg}^{i+1})$, and it can take any value in the range [0, π]

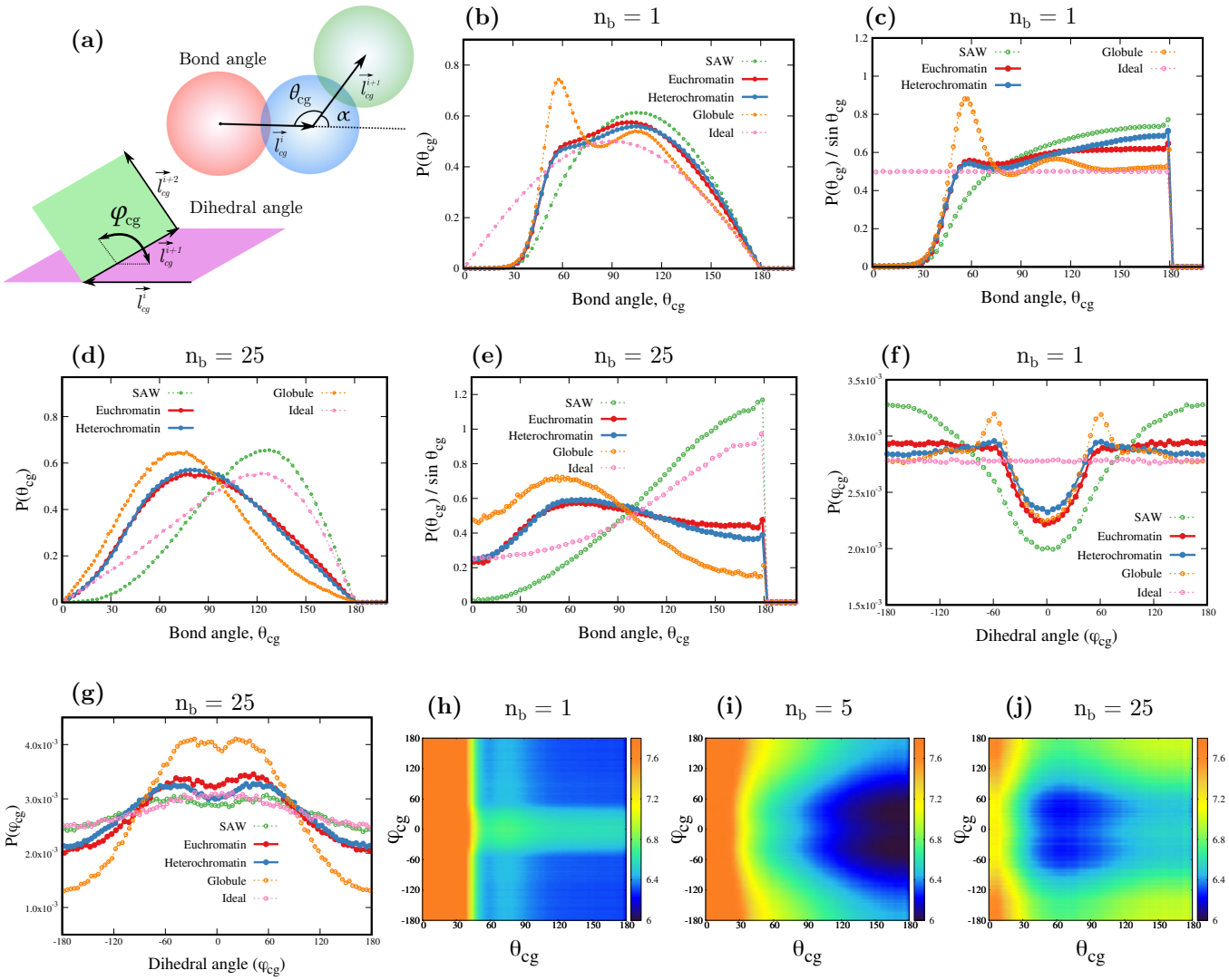

FIG. 4: (a) Schematic showing the bond angle $\theta_{\rm cg}$ and dihedral angle $\phi_{\rm cg}$ between coarse-grained beads. Distribution of angles for different epigenetic states, for the fine-grained model ($n_b = 1$) with nucleosome-linker (200bp) resolution (b) $P(\theta_{\rm cg})$, and (c) the distribution with a different measure $P(\theta_{\rm cg})/\sin(\theta_{\rm cg})$ are shown. Similar angle distribution for the coarse-grained chromatin model with one bead representing 5kb ($n_b = 25$) of chromatin are shown in (d) $P(\theta_{\rm cg})$ and (e)$P(\theta_{\rm cg})/\sin(\theta_{\rm cg})$. The distribution of dihedral angles for different epigenetic states for (f) the fine-grained model ($n_b = 1$) and (g) coarse-grained chromatin with one bead representing 5kb ($n_b = 25$) of chromatin. ($\theta_{\rm cg}$- $\phi_{\rm cg}$) energy plot for the euchromatic region for (h) the fine-grained model ($n_b = 1$), (i) CG chromatin with one bead representing 1kb chromatin ($n_b = 5$) and (j) CG chromatin with one bead representing 5kb chromatin ($n_b = 25$).

(see SI). As a control, we computed the angle and its distribution for an ideal chain, and our results match well with the known analytical answer [72] for $P(\theta_{cg})$ for different coarse-graining sizes (Fig. S4(c)). Then we computed the distribution of angles $P(\theta_{cg})$ for chromatin segments in different epigenetic states. As shown in Fig. 4(b), for an ideal chain, even with no coarse-graining ($n_b = 1$), the distribution has a shape given by $P(\theta_{cg}) = \sin(\theta_{cg})$ [72, 75]. This is due to the geometric measure, and it implies that when $\theta_{\rm cg}$ is near 90°, a large number of configurations are possible (having different azimuthal angles), while there is only one possible configuration for extreme cases if $\theta_{cg} = 0°$ and $\theta_{cg} = 180°$. Hence, to have a better understanding of the system, we also plot the corresponding probability density defined as $\tilde{P}(\theta_{cg}) = P(\theta_{cg})/\sin(\theta_{cg})$ in Fig. 4(c). For the ideal chain, with $n_b = 1$, $P(\theta_{cg})/\sin(\theta_{cg})$ is a flat curve (uniform distribution) reiterating the fact that the ideal chain is unbiased, and all configurations are equally likely. For SAW, the excluded volume would ensure that configurations with $\theta_{cg} \approx 0$ are not possible, and there is a natural bias towards extended configurations ($\theta_{cg} > 90°$).

Emergence of preferred inter-nucleosome angle from folded chromatin configurations: Our results here describe angle distribution for different types of chromatin segments. For fine-grained ($n_b = 1$) euchromatin and heterochromatin, deviating from the ideal chain and SAW behavior, a new peak emerges near $\theta_{cg} \approx 60°$ (Fig. 4(b)). Since we do not impose any preferred angle in the fine-grained model, this population with angles near 60° emerges purely from the packaging, based on the contact probability map. To understand this better, we deconvoluted the $P(\theta_{cg})$ distribution and represented it as a sum of two Gaussian distributions giving us two populations having mean values near $\approx 60°$ and $\approx 110°$ (Fig. S5(a)). Comparing the widths of the two populations suggests that the distribution with mean $\approx 60°$ is 2-3 times stiffer than the population with mean $\approx 110°$. For the highly folded globule (polymer with uniform LJ, $\epsilon = 1k_B$T), the peak at $\approx 60°$ is even more prominent, suggesting that tighter packaging could result in the population with $\approx 60°$ inter-nucleosome angles dominating the configurations. In contrast to the prevalent notion of smaller angles around $\approx 60°$, our analysis shows that, at least in the case of mESC chromatin, there is a prominent signature of two sub-populations—one highly folded and one extended (Fig 4(b) and (c)).

Next, we examined the angle distribution of a coarse-grained chromatin polymer (Fig 4(d) and (e)). A lesser-discussed fact about polymers (even for the ideal chain) is that, when coarse-graining is performed ($n_b > 1$), the angle distribution gains a bias (or a shift), with a preference emerging for the larger $\theta_{\rm cg}$ angles ($\theta_{\rm cg} > 90°$) (See [72, 75] and Fig. S4(c)). The SAW polymer has an extra bias towards extended angles as smaller angles are disfavored due to excluded volume effects.

For coarse-gained chromatin, the angle distributions deviate a lot from the ideal chain and SAW, displaying a preferred intrinsic angle in the range $\theta^0_{cg} \approx 50°$–$90°$ for a coarse-graining scale of 5kb (Fig 4(d,e)). For euchromatin, consistent with ideal chain and SAW, coarse-graining initially shifts the angle distribution towards larger angles (see $n_b = 5$ in Fig. S5(b)). However, for larger coarse-graining, long-range intra-chromatin interactions, such as TAD-forming loops, fold chromatin and shift the distribution towards smaller angles. For heterochromatin, presumably due to higher intra-chromatin interaction, the shift towards smaller angles occurs at $n_b = 5$ itself (Fig. S5(c)).

The effect of coarse-graining and deviation from ideal/SAW chain behavior is visible in $\tilde{P}(\theta_{cg})$ distribution as well (Fig. 4(e)). While the direct experimental readout of angles (e.g., via imaging) would yield $P(\theta_{cg})$, the scaled $\tilde{P}(\theta_{cg})$ is what would be useful for simulations; one can define an effective bond angle potential $V(\theta_{cg}) = -k_BT \log \tilde{P}(\theta_{cg})$ [75]. The $V(\theta_{cg})$ curves for chromatin segments have well-defined minima at preferred angles that depends on the coarse-graining scale, n_b (Fig. S6). One can also compute the effective bending "stiffness" of chromatin segments by comparing the inverse of the standard deviation, around the local maxima of $\tilde{P}(\theta_{cg})$ or by equating $V(\theta_{cg}) = \frac{k_b}{2}(1+cos(\theta_{cg}-\theta^0_{cg}))$. We find that bending stiffness is of the order of thermal energy $k_b \approx k_BT$ for all coarse-graining scales. This suggests that the chromatin polymer is not highly stiff and explores a wide range of angles. This is consistent with the emerging notion that chromatin is highly dynamic [76–79], and has high cell-to-cell variability.

We examined how the angles vary along the genomic locations. Similar to R_g and $l_{\rm cg}$, angles too have heterogeneity along the genome (Figs. 2(c) and S5(d)). A comparison of the average angle for different genomic locations reveals that there are higher angles near TAD boundaries/inter-TAD regions and lower angles in the interior of the TAD. This spatial variation of chromatin properties could be important for understanding and reconstructing chromatin configurations.

Dihedral angle distribution: The distributions of the dihedral angles $P(\phi_{\rm cg})$ for different chromatin/polymer segments for fine-grained ($n_b = 1$) and coarse-grained ($n_b = 25$) level are shown in Fig. 4(f–g). For the fine-grained model ($n_b = 1$), the ideal chain (control) has a uniform angle distribution as expected; the SAW polymer has a dip near $\phi = 0$ indicating self-avoidance/steric hindrance (Fig 4(f)). Even for an ideal chain, the coarse-graining leads to non-trivial changes in the ϕ distribution where a preference for smaller dihedral angles arises. For the fine-grained chromatin and globule, due to high folding, the probability of obtaining smaller angles (ϕ near zero) increases, and larger angles become rarer compared with the SAW polymer. Folding also leads to a peak near $\phi \approx 60°$, which is prominent for the globule.

A preference for smaller ϕ values appears on coarse-graining, similar to the Ideal chain. At the same time, the folding via long-range intra-chromatin interactions results in the formation of peaks near $\phi \approx \pm 60°$. Both of these effects together define the coarse-grained ϕ distributions (Fig. 4(g)). Similar to the bending angle distribution, the dihedral angle distributions too are very broad, implying a weak angle stiffness.

Similar to $V(\theta_{\rm cg})$, we define an effective dihedral potential $V(\phi_{cg}) = -k_BT \log P(\phi_{cg})$ (see Fig. S7). Assuming that the distributions of $\theta_{\rm cg}$ and $\phi_{\rm cg}$ are independent, we have plotted the heatmap of $V(\theta_{cg}, \phi_{cg}) = V(\theta_{cg}) + V(\phi_{cg})$ in the ($\theta_{\rm cg}$ – $\phi_{\rm cg}$) plane (see Fig 4(h–j)). Here the color-bar represents the energy $V(\theta_{cg}, \phi_{cg})$ values in $k_{\rm B}$T units. For the fine-grained model low values of $\theta_{\rm cg}$ and $\phi_{\rm cg}$ are penalized due to self-avoidance (Fig. 4(h)). This effect reduces with coarse-graining. For lower coarse-graining, higher $\theta_{\rm cg}$ and intermediate $\phi_{\rm cg}$ values are preferred (Fig. 4(i)), while for higher coarse-graining $\theta_{\rm cg}$ in the range 50°–90° and $\phi_{\rm cg}$ values close to ±60° are favored (Fig. 4(j)). This again shows that angle preferences for chromatin are scale-dependent—depending on the coarse-graining scale, the preferred values vary considerably.

Simulating a coarse-grained chromatin

This work provides systematic estimates of the size of coarse-grained beads, their fluctuations, the overlap among the beads due to the mixing of the polymer segments, and the distribution of both bond and dihedral angles. Here we integrate these quantities to simulate a coarse-grained chromatin polymer and examine their relevance.

We simulated a 100 beads long coarse-grained bead-spring polymer of a total length of 500kb, with each bead representing 5kb of chromatin. The values of the diameter of the 5kb bead ($\sigma = l_{cg} = 107$nm, for $n_b = 25$) and the spring constant ($K_{cg} = 2.4pN/\mu m = 7k_B\mathrm{T}/l_{cg}^2$) are taken from Fig. 3(c) and (h), respectively. To incorporate the observed overlap between chromatin segments, non-bonded bead pairs in the polymer interact via a Lennard-Jones-like potential with extra softness, available in LAMMPS (see Sec. S1.C). In this soft LJ potential, the overlap is controlled by a parameter λ ($1 \geq \lambda > 0$), with $\lambda = 1$ resulting in full LJ potential, and $\lambda \to 0$ causing highly overlapping soft interaction (Fig. 5(a)). It also has an interaction parameter ϵ (similar to LJ) that controls the depth of the potential. We simulated the polymer by varying these two parameters λ and ϵ. In Fig. 5(b), we plot R_g of the 500kb chromatin as a function of the softness parameter λ for various values of the interaction parameter ϵ. Depending on the (λ, ϵ) values, we can achieve R_g values that are comparable to what is observed experimentally (shaded region). The rough estimate of the approximate radius obtained from the microscopy image of $\approx$ 500 kb region in Szabo et al. [38] is shown as the horizontal shaded region.

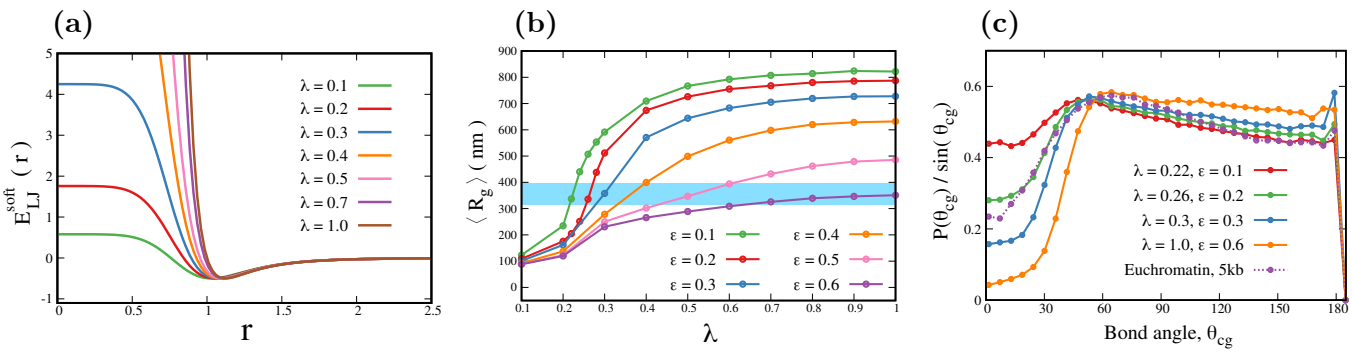

FIG. 5: (a) Soft-LJ potential for various values of softness parameter λ at fixed value of $\epsilon = 0.5$. (b) Average R_g computed as a function of the softness parameter (λ), that controls the overlap between the polymer beads, for various values of interaction strength ϵ. The polymer with different interaction strengths ϵ show similar R_g values as observed in experiments (shaded region) at different levels of softness λ. (c) The distribution $P(\theta_{\mathrm{cg}})/\sin(\theta_{\mathrm{cg}})$ for representative values of λ and ϵ, that give the R_g of same order as observed in experiments, is compared with the distribution for the coarse-grained ($n_b = 25$, 5kb) euchromatic region (purple color).

Fig. 5(b) shows that, if we assume uniform interaction among all beads, one requires some amount of softness to obtain experimentally reasonable R_g values for small ϵ. One could argue that using the LJ potential with high interaction strength ($\epsilon = 0.6$) and no extra softness ($\lambda = 1.0$) can result in smaller R_g values and, therefore, achieve a similar effect as obtained by using the soft potential. However, the crucial point is that ϵ is not a completely free parameter. The interaction strength would influence other properties of the polymer, such as angle distribution and contact probability. To test the appropriate value of the ϵ parameter, we computed the angle distribution for different cases relevant here. Fig. 5(c) shows the angle distribution $P(\theta_{\mathrm{cg}})/\sin(\theta_{\mathrm{cg}})$ for four representative pairs of λ and ϵ values ($(\lambda = 0.22, \epsilon = 0.1), (\lambda = 0.26, \epsilon = 0.2), (\lambda = 0.3, \epsilon = 0.3)$, and $(\lambda = 1, \epsilon = 0.6)$) that match with the experimental R_g. We compared these distributions with the angle distribution obtained for the coarse-grained euchromatin region at 5kb ($n_b = 25$) resolution (purple curve) taken from Fig. 4(e). Even though different ϵ and λ values give similar R_g, they do not show similar angle distributions. When LJ with higher interaction strength ($\epsilon = 0.6k_B\mathrm{T}$) and no extra softness ($\lambda = 1$) is used, the angle distribution underestimates the probability for smaller angles (orange curve). On the other hand, LJ with small interaction strength ($\epsilon = 0.1k_B\mathrm{T}$) and very high softness ($\lambda = 0.22$) overestimates the probability for smaller angles (red curve). It appears that there is an optimal interaction strength ($\epsilon = 0.2k_B\mathrm{T}$) and softness ($\lambda = 0.26$) that gives the best match with the coarse-grained euchromatin (green and purple curves).

Comparing all the four distributions, it can be concluded that the closest approximation for the euchromatin is obtained for a soft potential with $\lambda = 0.26$ and $\epsilon = 0.2k_B\mathrm{T}$. This parameter combination gives both the angle distribution as well as R_g value comparable to what is expected for a chromatin polymer. This reiterates the relevance of overlap in coarse-grained models. The lack of overlap would lead to over-estimation R_g or equivalently 3D distance values. Typically, chromatin simulations compute R_g in dimensionless units and estimate bead diameter as a fitting parameter. The lack of overlap can result in an under-estimation of the bead diameter.

Note that in reality, the inter-bead interaction strengths (even within a TAD) are likely to be non-uniform since the contact probability is heterogeneous[66]. The existing estimates indicate that there are many weak interactions (small ϵ) and a few strong interactions (large ϵ)[66]. Reconciling this abundance of weak interactions with our coarse-grained simulation results above, we see that one must necessarily incorporate softness in the inter-bead interactions to predict chromatin 3D distances accurately.

Conclusion

In this work, we address a fundamental question in modeling chromatin: what are the properties and parameters of a coarse-grained chromatin polymer, and how do they vary in a scale-dependent manner? To answer this, we made use of the recently published Micro-C contact map for mESCs and constructed an ensemble of chromatin configurations at 200bp resolution consistent with the map. We then systematically coarse-grained the chromatin and predicted properties and parameters of a coarse-grained bead spring chain. Our findings estimate the mean values of physical dimensions, bond angles, and dihedral angles of the coarse-grained chromatin and their distributions, giving an idea about the stretching and bending stiffness of the chromatin polymer. Our work further shows the effect of chromatin heterogeneity along the polymer contour, finding that TAD interior and TAD boundary have different coarse-grained bead dimensions and average angle values. Contrary to the prevalent notion, our results show that coarse-grained chromatin beads should be modeled as soft particles that can overlap.

Our results are significant for everyone making chromatin polymer models to interpret chromatin confirmation experiments or to simulate chromatin organization and dynamics. Since existing models start with a coarse-grained picture, a systematic procedure, as we presented here, is a necessity to make physically sensible predictions. Since we know the dimension and properties of a nucleosome and linker DNA, the only way to study this is to start with a fine-grained model at near-nucleosome resolution. The recent publication of the Micro-C data allowed us to do this.

It must be stated that the whole of our analysis is based on the Micro-C data for the mESCs from Hsieh et al. [33]. Hence the numbers emerging from this study would represent embryonic cell chromatin. In the future, analysis can be further extended to study various other cell types as new data emerge.

Acknowledgment

RP Acknowledges useful discussions with Xavier Darzacq, Leonid Mirny, Daniel Jost, Geeta Narlikar, and Marc Marti-Renom. We acknowledge useful discussions with Vladimir Teif, Mayuri Rege, PB Sunil Kumar, Madan Rao, and Gaurav Bajpai. SK acknowledges fellowship support from the CSIR, India, and KK acknowledges iPDF support from IIT Bombay. We acknowledge funding from the Department of Biotechnology, India (Grant number: BT/HRD/NBA/39/12/2018-19). We also acknowledge the National Supercomputing Mission (NSM) for providing computing resources of 'PARAM Brahma' at IISER Pune, which is implemented by C-DAC and supported by the Ministry of Electronics and Information Technology (MeitY) and Department of Science and Technology (DST), Government of India.

---

[1] B. Alberts, Molecular Biology of The Cell (Garland Science, Taylor and Francis Group, New York, 2014), 6th ed.
[2] W. A. Bickmore, Annu. Rev. Genomics Hum. Genet. **14**, 67 (2013).
[3] R. D. Kornberg and Y. Lorch, Cell **98**, 285 (1999).
[4] M. J. Rowley and V. G. Corces, Nature Reviews Genetics **19**, 1 (2018), ISSN 1471-0056, URL `http://www.nature.com/articles/s41576-018-0060-8`.
[5] C. B. Hug and J. M. Vaquerizas, Trends in Genetics **34**, 903 (2018).
[6] H. K. Long, S. L. Prescott, and J. Wysocka, Cell **167**, 1170 (2016).
[7] B. Bonev and G. Cavalli, Nature Reviews Genetics **17**, 661 (2016).
[8] A. D. Stephens, E. J. Banigan, and J. F. Marko, Current opinion in cell biology **58**, 76 (2019).
[9] M. Di Stefano, J. Paulsen, D. Jost, and M. A. Marti-Renom, Curr. Opin. Genet. Dev. **67**, 25 (2021).
[10] L. Giorgetti, R. Galupa, E. P. Nora, T. Piolot, F. Lam, J. Dekker, G. Tiana, and E. Heard, Cell **157**, 950 (2014).
[11] M. Di Pierro, B. Zhang, E. L. Aiden, P. G. Wolynes, and J. N. Onuchic, PNAS **113**, 12168 (2016).
[12] Q. MacPherson, B. Beltran, and A. J. Spakowitz, PNAS **115**, 12739 (2018).
[13] C. A. Brackley, J. M. Brown, D. Waithe, C. Babbs, J. Davies, J. R. Hughes, V. J. Buckle, and D. Marenduzzo, Genome biology **17**, 1 (2016).
[14] C. A. Brackey, D. Marenduzzo, and N. Gilbert, Nature Methods **17**, 767 (2020).

[15] G. Bajpai, D. A. Pavlov, D. Lorber, T. Volk, and S. Safran, Elife **10**, e63976 (2021).
[16] M. Falk, Y. Feodorova, N. Naumova, M. Imakaev, B. R. Lajoie, H. Leonhardt, B. Joffe, J. Dekker, G. Fudenberg, I. Solovei, et al., Nature **570**, 395 (2019).
[17] A. Goloborodko, J. F. Marko, and L. A. Mirny, Biophys. J. **110**, 2162 (2016).
[18] S. K. Ghosh and D. Jost, PLoS computational biology **14**, e1006159 (2018).
[19] S. Bianco, D. G. Lupiáñez, A. M. Chiariello, C. Annunziatella, K. Kraft, R. Schöpflin, L. Wittler, G. Andrey, M. Vingron, A. Pombo, et al., Nat. Genet. **50**, 662 (2018).
[20] G. Shi, L. Liu, C. Hyeon, and D. Thirumalai, Nat. Commun. **9**, 1 (2018).
[21] N. Ganai, S. Sengupta, and G. I. Menon, Nucleic Acids Res. **42**, 4145 (2014).
[22] K. Kumari, B. Duenweg, R. Padinhateeri, and J. R. Prakash, Biophys. J. **118**, 2193 (2020).
[23] D. Chatenay, S. Cocco, R. Monasson, D. Thieffry, and J. Dalibard, Multiple Aspects of DNA and RNA: from Biophysics to Bioinformatics: Lecture Notes of the Les Houches Summer School 2004 (Elsevier, 2005).
[24] C. Bustamante, Z. Bryant, and S. B. Smith, Nature **421**, 423 (2003).
[25] J. F. Marko and S. Cocco, Physics World **16**, 37 (2003).
[26] M. Mir, W. Bickmore, E. E. Furlong, and G. Narlikar, Development **146**, dev182766 (2019).
[27] S. L. Klemm, Z. Shipony, and W. J. Greenleaf, Nature Reviews Genetics **20**, 207 (2019).
[28] E. Lieberman-Aiden, N. L. Van Berkum, L. Williams, M. Imakaev, T. Ragoczy, A. Telling, I. Amit, B. R. Lajoie, P. J. Sabo, M. O. Dorschner, et al., Science **326**, 289 (2009).
[29] E. P. Nora, B. R. Lajoie, E. G. Schulz, L. Giorgetti, I. Okamoto, N. Servant, T. Piolot, N. L. van Berkum, J. Meisig, J. Sedat, et al., Nature **485**, 381 (2012).
[30] J. R. Dixon, S. Selvaraj, F. Yue, A. Kim, Y. Li, Y. Shen, M. Hu, J. S. Liu, and B. Ren, Nature **485**, 376 (2012).
[31] S. S. Rao, M. H. Huntley, N. C. Durand, E. K. Stamenova, I. D. Bochkov, J. T. Robinson, A. L. Sanborn, I. Machol, A. D. Omer, E. S. Lander, et al., Cell **159**, 1665 (2014).
[32] T.-H. S. Hsieh, A. Weiner, B. Lajoie, J. Dekker, N. Friedman, and O. J. Rando, Cell **162**, 108 (2015).
[33] T.-H. S. Hsieh, C. Cattoglio, E. Slobodyanyuk, A. S. Hansen, O. J. Rando, R. Tjian, and X. Darzacq, Molecular cell **78**, 539 (2020).
[34] N. Krietenstein and O. J. Rando, Current Opinion in Genetics & Development **61**, 32 (2020).
[35] R. Jäger, G. Migliorini, M. Henrion, R. Kandaswamy, H. E. Speedy, A. Heindl, N. Whiffin, M. J. Carnicer, L. Broome, N. Dryden, et al., Nature communications **6**, 1 (2015).
[36] V. Ramani, D. A. Cusanovich, R. J. Hause, W. Ma, R. Qiu, X. Deng, C. A. Blau, C. M. Disteche, W. S. Noble, J. Shendure, et al., Nature protocols **11**, 2104 (2016).
[37] S. G. Swygert, S. Kim, X. Wu, T. Fu, T.-H. Hsieh, O. J. Rando, R. N. Eisenman, J. Shendure, J. N. McKnight, and T. Tsukiyama, Molecular Cell **73**, 533 (2019).
[38] Q. Szabo, A. Donjon, I. Jerković, G. L. Papadopoulos, T. Cheutin, B. Bonev, E. P. Nora, B. G. Bruneau, F. Bantignies, and G. Cavalli, Nat. Genet. **52**, 1151 (2020).
[39] R. Imai, T. Nozaki, T. Tani, K. Kaizu, K. Hibino, S. Ide, S. Tamura, K. Takahashi, M. Shribak, and K. Maeshima, Mol. Biol. Cell **28**, 3349 (2017).
[40] K. Maeshima, S. Ide, and M. Babokhov, Current Opinion in Cell Biology **58**, 95 (2019), ISSN 0955-0674, cell Nucleus, URL `http://www.sciencedirect.com/science/article/pii/S0955067418301881`.
[41] M. Eltsov, D. Grewe, N. Lemercier, A. Frangakis, F. Livolant, and A. Leforestier, Nucleic acids research **46**, 9189 (2018).
[42] H. D. Ou, S. Phan, T. J. Deerinck, A. Thor, M. H. Ellisman, and C. C. O'Shea, Science **357**, 1 (2017), ISSN 0036-8075, URL `http://science.sciencemag.org/content/357/6349/eaag0025/tab-pdf`.
[43] A. N. Boettiger, B. Bintu, J. R. Moffitt, S. Wang, B. J. Beliveau, G. Fudenberg, M. Imakaev, L. A. Mirny, C.-t. Wu, and X. Zhuang, Nature **529**, 418 (2016).
[44] H. A. Shaban, R. Barth, L. Recoules, and K. Bystricky, Genome biology **21**, 1 (2020).
[45] J. J. Parmar, M. Woringer, and C. Zimmer, Annual Review of Biophysics **48**, 231 (2019), ISSN 1936-122X.
[46] J. Dekker, K. Rippe, M. Dekker, and N. Kleckner, science **295**, 1306 (2002).
[47] Y. Nishino, M. Eltsov, Y. Joti, K. Ito, H. Takata, Y. Takahashi, S. Hihara, A. S. Frangakis, N. Imamoto, T. Ishikawa, et al., The EMBO Journal **31**, 1644 (2012), https://www.embopress.org/doi/pdf/10.1038/emboj.2012.35, URL `https://www.embopress.org/doi/abs/10.1038/emboj.2012.35`.
[48] D. Jost, P. Carrivain, G. Cavalli, and C. Vaillant, Nucleic Acids Res. **42**, 9553 (2014).
[49] J. Huertas, E. J. Woods, and R. Collepardo-Guevara, Current Opinion in Cell Biology **75**, 102067 (2022).
[50] G. Fudenberg, M. Imakaev, C. Lu, A. Goloborodko, N. Abdennur, and L. A. Mirny, Cell Rep. **15**, 2038 (2016).
[51] J. J. Parmar and R. Padinhateeri, Curr. Opin. Struct. Biol. **64**, 111 (2020).
[52] G. D. Bascom, C. G. Myers, and T. Schlick, PNAS **116**, 4955 (2019).
[53] A. Rosa and R. Everaers, PLoS Comput. Biol. **4**, e1000153 (2008).
[54] C. T. Clarkson, E. A. Deeks, R. Samarista, H. Mamayusupova, V. B. Zhurkin, and V. B. Teif, Nucleic Acids Res. **47**, 11181 (2019).
[55] M. Conte, L. Fiorillo, S. Bianco, A. M. Chiariello, A. Esposito, and M. Nicodemi, Nat. Commun. **11**, 1 (2020).
[56] Y. Qi and B. Zhang, PLoS Comput. Biol. **15**, e1007024 (2019).
[57] G. Bajpai and R. Padinhateeri, Biophys. J. **118**, 207 (2020).
[58] H. Tjong, W. Li, R. Kalhor, C. Dai, S. Hao, K. Gong, Y. Zhou, H. Li, X. J. Zhou, M. A. Le Gros, et al., Proceedings of the National Academy of Sciences **113**, E1663 (2016).
[59] N. Hua, H. Tjong, H. Shin, K. Gong, X. J. Zhou, and F. Alber, Nature protocols **13**, 915 (2018).

[60] G. Tiana, A. Amitai, T. Pollex, T. Piolot, D. Holcman, E. Heard, and L. Giorgetti, Biophysical journal **110**, 1234 (2016).
[61] M. M. Tortora, H. Salari, and D. Jost, Current opinion in genetics & development **61**, 37 (2020).
[62] M. Ohno, T. Ando, D. G. Priest, V. Kumar, Y. Yoshida, and Y. Taniguchi, Cell **176**, 520 (2019).
[63] R. Collepardo-Guevara and T. Schlick, Proceedings of the National Academy of Sciences **111**, 8061 (2014), ISSN 0027-8424, https://www.pnas.org/content/111/22/8061.full.pdf, URL `https://www.pnas.org/content/111/22/8061`.
[64] S. E. Farr, E. J. Woods, J. A. Joseph, A. Garaizar, and R. Collepardo-Guevara, Nature communications **12**, 1 (2021).
[65] S. A. Grigoryev, Biophysical journal **114**, 2290 (2018).
[66] K. Kumari, J. R. Prakash, and R. Padinhateeri, Biophysical Journal (2022).
[67] A. M. Chiariello, S. Bianco, A. M. Oudelaar, A. Esposito, C. Annunziatella, L. Fiorillo, M. Conte, A. Corrado, A. Prisco, M. S. Larke, et al., Cell Reports **30**, 2125 (2020).
[68] G. Forte, A. Buckle, S. Boyle, D. Marenduzzo, N. Gilbert, and C. A. Brackley, bioRxiv (2021).
[69] S. Plimpton, Journal of computational physics **117**, 1 (1995).
[70] G. Bajpai, I. Jain, M. M. Inamdar, D. Das, and R. Padinhateeri, PLoS computational biology **13**, e1005365 (2017).
[71] J. M. Brown, N. A. Roberts, B. Graham, D. Waithe, C. Lagerholm, J. M. Telenius, S. De Ornellas, A. M. Oudelaar, C. Scott, I. Szczerbal, et al., Nature communications **9**, 1 (2018).
[72] M. Laso, H. Öttinger, and U. Suter, The Journal of chemical physics **95**, 2178 (1991).
[73] Y. Cui and C. Bustamante, Proceedings of the National Academy of Sciences **97**, 127 (2000).
[74] M. G. Poirier and J. F. Marko, Proceedings of the National Academy of Sciences **99**, 15393 (2002).
[75] T. Vettorel, G. Besold, and K. Kremer, Soft Matter **6**, 2282 (2010).
[76] A. S. Hansen, C. Cattoglio, X. Darzacq, and R. Tjian, Nucleus **9**, 20 (2018).
[77] E. I. Prieto and K. Maeshima, Essays in biochemistry **63**, 133 (2019).
[78] M. Gabriele, H. B. Brandão, S. Grosse-Holz, A. Jha, G. M. Dailey, C. Cattoglio, T.-H. S. Hsieh, L. Mirny, C. Zechner, and A. S. Hansen, Science **376**, 496 (2022).
[79] A. S. Hansen, I. Pustova, C. Cattoglio, R. Tjian, and X. Darzacq, elife **6**, e25776 (2017).